Genes to Cells

WILEY

Genes to Cells

ORIGINAL ARTICLE OPEN ACCESS

Alternative Splicing of *FBLN2* Generates a Prometastatic Extracellular Matrix in Gastrointestinal Cancers by Determining N-Glycosylation of Fibulin 2

Ryo Funayama[1,2] | Yujue Wang[1,3] | Masaki Hosogane[1] | Wei-Chen Kao[1] | Shingo Toyama[4] | Masahiro Ohira[1] | Masaki Matsumoto[5] | Takashi Aizawa[4] | Minoru Kobayashi[4] | Hideaki Karasawa[4] | Shinobu Ohnuma[4] | Keiichi I. Nakayama[2,6] | Michiaki Unno[4] | Keiko Nakayama[1,7]

[1]Department of Cell Proliferation, ART, Graduate School of Medicine, Tohoku University, Sendai, Japan | [2]Anticancer Strategies Laboratory, Advanced Research Initiative, Institute of Science Tokyo, Tokyo, Japan | [3]Department of Cellular Function, Graduate School of Life Sciences, Tohoku University, Sendai, Japan | [4]Department of Surgery, Graduate School of Medicine, Tohoku University, Sendai, Japan | [5]Department of Omics and Systems Biology, Graduate School of Medical and Dental Sciences, Niigata University, Niigata, Japan | [6]Department of Molecular and Cellular Biology, Medical Institute of Bioregulation, Kyushu University, Fukuoka, Japan | [7]Research Infrastructure Management Center, Institute of Science Tokyo, Tokyo, Japan

Correspondence: Keiko Nakayama (nakayama.keiko@tmd.ac.jp) | Ryo Funayama (funayama.ryo@tmd.ac.jp)

Received: 11 March 2025 | **Revised:** 19 April 2025 | **Accepted:** 13 May 2025

Transmitting Editor: Hidenori Ichijo

Funding: This study was supported by Japan Society for the Promotion of Science (JSPS) KAKENHI grants JP20K07560, JP23K06626, and JP25K10462 (to R.F.) as well as JP17H04035, JP18H05215, JP21H02458, and JP24K02300 (to K.N.).

Keywords: alternative splicing | extracellular matrix | fibulin 2 | gastrointestinal cancers | glycosylation

ABSTRACT

Fibulin 2 (FBLN2) is an extracellular matrix glycoprotein. Exclusion of exon 9 of *FBLN2* is one of the most recurrent splicing events across multiple types of cancer, but its functional relevance in cancer has remained unexplored. We here reveal that the exclusion of exon 9 of *FBLN2* results in the loss of a single N-glycosylation site that leads to misfolding of the FBLN2 protein as well as to a reduction in both its stability and secretion efficiency. Indeed, the extracellular matrix of human colorectal cancer tissue exhibits a reduced abundance of FBLN2. This deficiency of FBLN2 together with a concomitant increase in the abundance of fibronectin 1 in the tumor microenvironment promotes the adhesion and migration of colorectal cancer cells. Our data thus suggest that the alternative splicing of *FBLN2* exon 9 generates a prometastatic extracellular environment in cancer tissue by determining FBLN2 glycosylation.

1 | Introduction

Extracellular matrix (ECM) consisting of noncellular components of the tumor microenvironment (TME) accounts for up to 60% of tumor mass (Henke et al. 2019; Anderson and Simon 2020). This ECM is composed of various fibrous proteins including fibrillar collagens, fibronectin 1 (FN1), and fibulin 2 (FBLN2) (Brassart-Pasco et al. 2020; Cox 2021). Although many cell types contribute to the production of ECM proteins in tumor tissue, fibroblasts are the major source for ECM deposition (DeLeon-Pennell et al. 2020; Winkler et al. 2020; Belhabib et al. 2021). The meshwork architecture of ECM provides a scaffold for tumor cells to proliferate, migrate, and escape immune surveillance (Pickup et al. 2014; Kai et al. 2019). Given that the

Ryo Funayama, Yujue Wang, and Masaki Hosogane contributed equally to this work.

This is an open access article under the terms of the Creative Commons Attribution-NonCommercial-NoDerivs License, which permits use and distribution in any medium, provided the original work is properly cited, the use is non-commercial and no modifications or adaptations are made.

© 2025 The Author(s). *Genes to Cells* published by Molecular Biology Society of Japan and John Wiley & Sons Australia, Ltd.

ECM in normal tissue restricts abnormal cell proliferation and migration, changes in the composition, abundance, and three-dimensional architecture of ECM—so-called ECM remodeling—are required for a tumor to develop and spread (Mohan et al. 2020; Rafaeva and Erler 2020; de Visser and Joyce 2023). ECM remodeling is driven by not only altered expression but also alternative splicing of ECM genes.

Transcripts of most ECM genes undergo extensive alternative splicing that results in the production of multiple protein variants from individual genes (Viloria and Hill 2016; Efthymiou et al. 2020). Such splice variants of ECM proteins may include different protein domains and posttranslational modification sites that affect protein function or abundance (Naba et al. 2016; Rekad et al. 2022). The expression of ECM splice variants has been associated with various diseases including cancer, implicating such variants in tumor progression as well as suggesting their potential as prognostic biomarkers of cancer (Chiquet-Ehrismann and Tucker 2011; Naba 2023). Although the precise functional properties of most ECM splice variants remain to be fully characterized, the alternative splicing of ECM genes may lead to the generation of a protumorigenic and prometastatic TME by increasing the complexity and diversity of ECM architecture (Efthymiou et al. 2020; Rekad et al. 2022).

FBLN2 is an ECM glycoprotein that harbors an array of calcium-binding epidermal growth factor (cbEGF)-like domains and a COOH-terminal fibulin-type module (Pan et al. 1993; Timpl et al. 2003). It is expressed in various tissues as a disulfide-linked homodimer and binds to a variety of ECM proteins including FN1, nidogen 1 (NID1), perlecan, and fibrillin 1 (Pan et al. 1993; Sasaki et al. 1995, 1997; Timpl et al. 2003). Although FBLN2 is dispensable for mouse development (Sicot et al. 2008), it is implicated in cancer progression in humans and mice (Zhang, Hui, et al. 2020; Mahajan et al. 2021). The expression of FBLN2 is reduced in breast cancer tissue compared with normal breast tissue (Yi et al. 2007), and its overexpression suppresses the motility and invasion of breast cancer cells without affecting cell proliferation in vitro, suggestive of a tumor-suppressive role of FBLN2. In contrast, increased release of FBLN2 and NID1 from enteric neurons was found to promote colorectal cancer (CRC) progression in NDRG4 (N-Myc downstream-regulated gene 4)-deficient mice (Vaes et al. 2021). Furthermore, FBLN2 is required for the growth and metastasis of lung adenocarcinoma cells in mice (Baird et al. 2013). This tumor-promoting ability of FBLN2 in lung adenocarcinoma is dependent on FBLN2 protein derived from tumor cells as opposed to surrounding stromal cells. FBLN2 thus appears to suppress or promote cancer progression in a manner dependent on the type or stage of cancer.

The human *FBLN2* gene encodes two alternative splice variants—variant 1 (v1, consensus coding sequence [CCDS] 46761.1) and variant 2 (v2, CCDS46762.1)—which include or exclude exon 9, respectively (Figure 1A, the exon numbering was based on the transcript v1 from RefSeq NM_001004019.2 in this study) (Grassel et al. 1999; Timpl et al. 2003). Given that exon 9 encodes a single cbEGF-like domain, FBLN2 v2 has one fewer cbEGF-like domain than does v1 (Timpl et al. 2003; de Vega et al. 2009). Analysis of The Cancer Genome Atlas (TCGA) RNA-sequencing (seq) data revealed that the exclusion of *FBLN2* exon 9 is one of the most recurrent splicing events across multiple cancer types (Danan-Gotthold et al. 2015; Sebestyen et al. 2015; Ryan et al. 2016). The functional relevance of *FBLN2* splicing in cancer has remained unexplored, however (Chu and Tsuda 2004; de Vega et al. 2009). We have now examined how the exclusion of exon 9 affects the expression and function of FBLN2 protein and investigated its contribution to tumor progression.

2 | Results

2.1 | Variant 2 Is the Major Splice Variant of FBLN2 Expressed in the Fibroblasts of Gastrointestinal Cancers

To validate and expand previous findings with regard to *FBLN2* splicing in cancer (Danan-Gotthold et al. 2015; Sebestyen et al. 2015), we examined the TCGASpliceSeq database, in which TCGA RNA-seq data are analyzed by SpliceSeq software to determine the mRNA splicing patterns of TCGA samples (Ryan et al. 2016). Among 33 cancer types included in TCGA, we selected 16 types that are accompanied by > 10 matched normal tissue samples as controls, and found that 13 cancer types showed a decrease in the inclusion of *FBLN2* exon 9 in the primary tumor relative to normal tissue (Figure 1B). The four most significant decreases were detected in gastrointestinal cancers, specifically in esophageal carcinoma (ESCA), colon adenocarcinoma (COAD), stomach adenocarcinoma (STAD), and rectum adenocarcinoma (READ) (Figure 1B,C). Furthermore, analysis of RNA-seq data (GSE50760) (Kim et al. 2014) for CRC tissue revealed that this splicing change was more pronounced in metastatic liver tumors than in the corresponding primary tumors (Figure 1D). Together, these data suggest that the exclusion of exon 9 might contribute to CRC metastasis.

To further validate the change in the splicing of *FBLN2* exon 9 in CRC, we performed reverse transcription (RT) and quantitative polymerase chain reaction (qPCR) analysis of primary tumors and adjacent normal tissue isolated from individuals with CRC. Variant-specific primers were used to distinguish *FBLN2* v1 and v2 mRNAs in qPCR analysis (Figure S1). Consistent with the RNA-seq data, RT-qPCR analysis revealed that the fraction of *FBLN2* v1 mRNA was reduced in primary tumor tissue relative to normal tissue (Figure 1E). These findings thus indicated that exon 9 is excluded from *FBLN2* mRNA in most cancer types, especially in gastrointestinal cancers, with v2 thus being the major FBLN2 splice variant in cancer tissue.

We evaluated the potential role of *FBLN2* splicing in determining the abundance of *FBLN2* mRNA using TCGA RNA-seq data for the 16 cancer types analyzed in Figure 1B. Although the amount of *FBLN2* mRNA tended to be reduced in tumor tissue relative to normal tissue, there was no correlation between the extent of splicing of *FBLN2* exon 9 and *FBLN2* mRNA abundance (Figure S2). This finding suggested that the splicing of *FBLN2* exon 9 likely does not influence the level of *FBLN2* mRNA.

We next explored which cell types of colorectal tissue are responsible for this change in *FBLN2* splicing. To identify the cell types

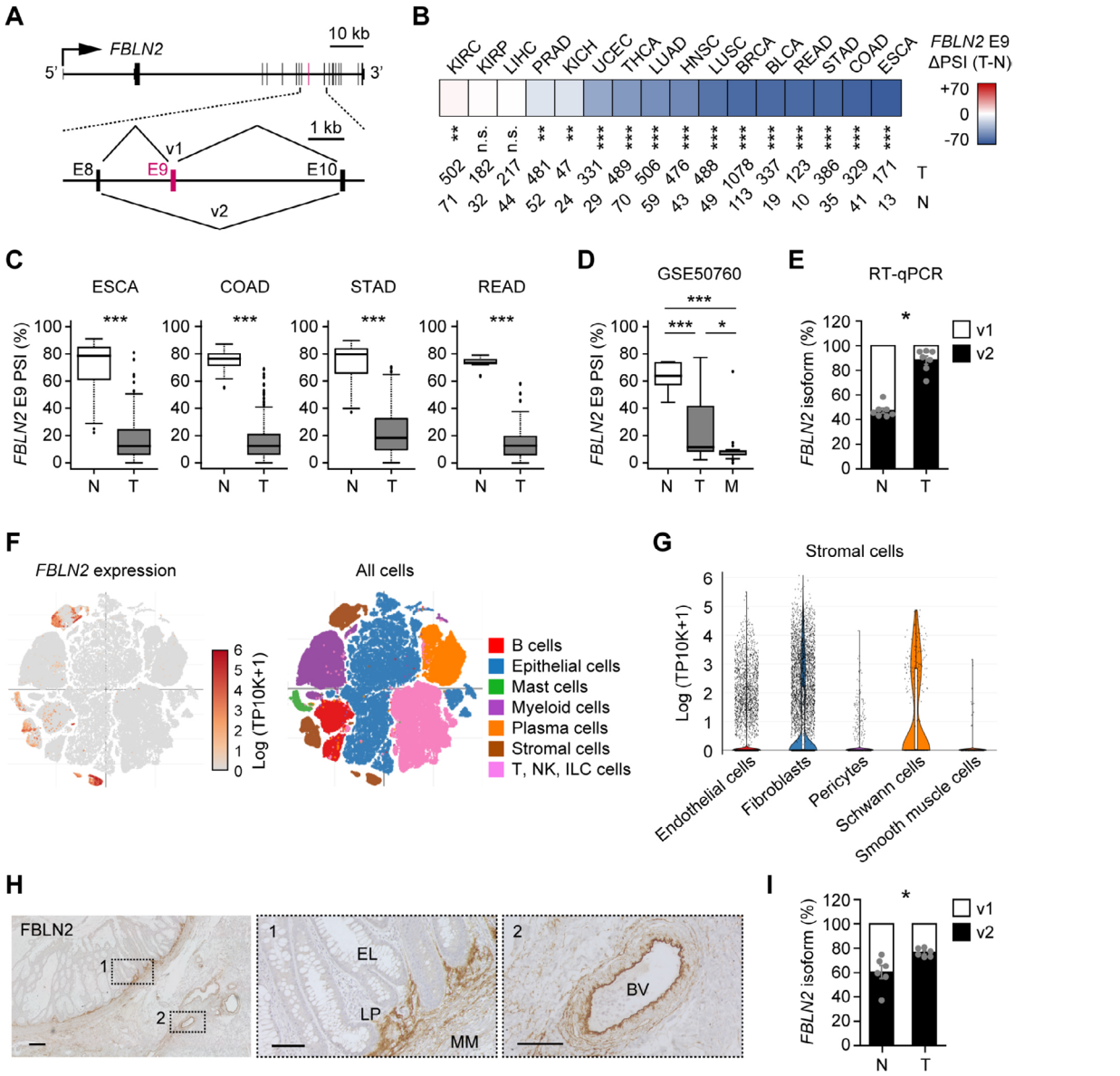

FIGURE 1 | Variant 2 is the major FBLN2 splice variant expressed in the fibroblasts of gastrointestinal cancers. (A) Schematic representation of the human *FBLN2* gene. Exon (E) 9 (magenta) is included or excluded in variant 1 (v1) or variant 2 (v2) mRNAs, respectively. (B) Difference in splicing of *FBLN2* exon 9 between normal (N) and primary tumor (T) tissue for 16 types of cancer in the TCGASpliceSeq database. Cancer type abbreviations are as in Table S2. PSI, percent spliced-in. The values at the bottom indicate the number of tumor (T) and normal (N) tissues examined. (C, D) Box plots for PSI values of *FBLN2* exon 9 determined from RNA-seq data for normal (N), primary tumor (T), or metastatic liver tumor (M) tissue for four selected cancer types in TCGA (C) or for CRC in GSE50760 (D). (E) RT-qPCR analysis of the expression of *FBLN2* v1 and v2 in normal and primary tumor tissue isolated from CRC patients. Data are means ± SEM ($n = 7$ patients). (F) Expression profiles for *FBLN2* in CRC tissue determined by scRNA-seq analysis (GSE178341). The color intensity in the left plot represents the abundance of *FBLN2* mRNA as shown by Log (TP10K + 1). TP10K + 1 indicates transcripts per 10 thousand plus one reads. The colors in the right plot correspond to cell identities. ILC, innate lymphoid cell; NK, natural killer. (G) Violin plots for the expression level of *FBLN2* in five stromal cell types determined by scRNA-seq analysis as in (F). (H) Representative immunohistochemical staining of FBLN2 in a tissue section containing normal epithelium isolated from a CRC patient. Boxed regions in the left image are shown at higher magnification in the middle and right images. BV, blood vessel; EL, epithelial layer; LP, lamina propria; MM, muscularis mucosae. Scale bars, 300 μm (left) and 100 μm (middle and right). (I) RT-qPCR analysis of *FBLN2* v1 and v2 expression in primary fibroblasts isolated from normal (N) or primary tumor (T) tissue of gastrointestinal cancer patients. Data are means ± SEM ($n = 6$ patients). *$p < 0.05$, **$p < 0.01$, ***$p < 0.001$, n.s. (not significant) by the Wilcoxon rank sum test followed by Benjamini–Hochberg correction for multiple testing (B, C), by one-way analysis of variance (ANOVA) followed by Tukey's post hoc test (D), or by the paired *t* test (E, I).

that express *FBLN2*, we analyzed single-cell (sc) RNA-seq data for CRC tissue (GSE178341) (Pelka et al. 2021). We found that *FBLN2* mRNA was present predominantly in stromal cells—in particular, in vascular endothelial cells and fibroblasts—rather than in epithelial cells, including cancer cells (Figure 1F,G). To confirm this finding, we performed immunohistochemical analysis of normal colorectal tissue surrounding tumors isolated from individuals with CRC. FBLN2 expression was detected in

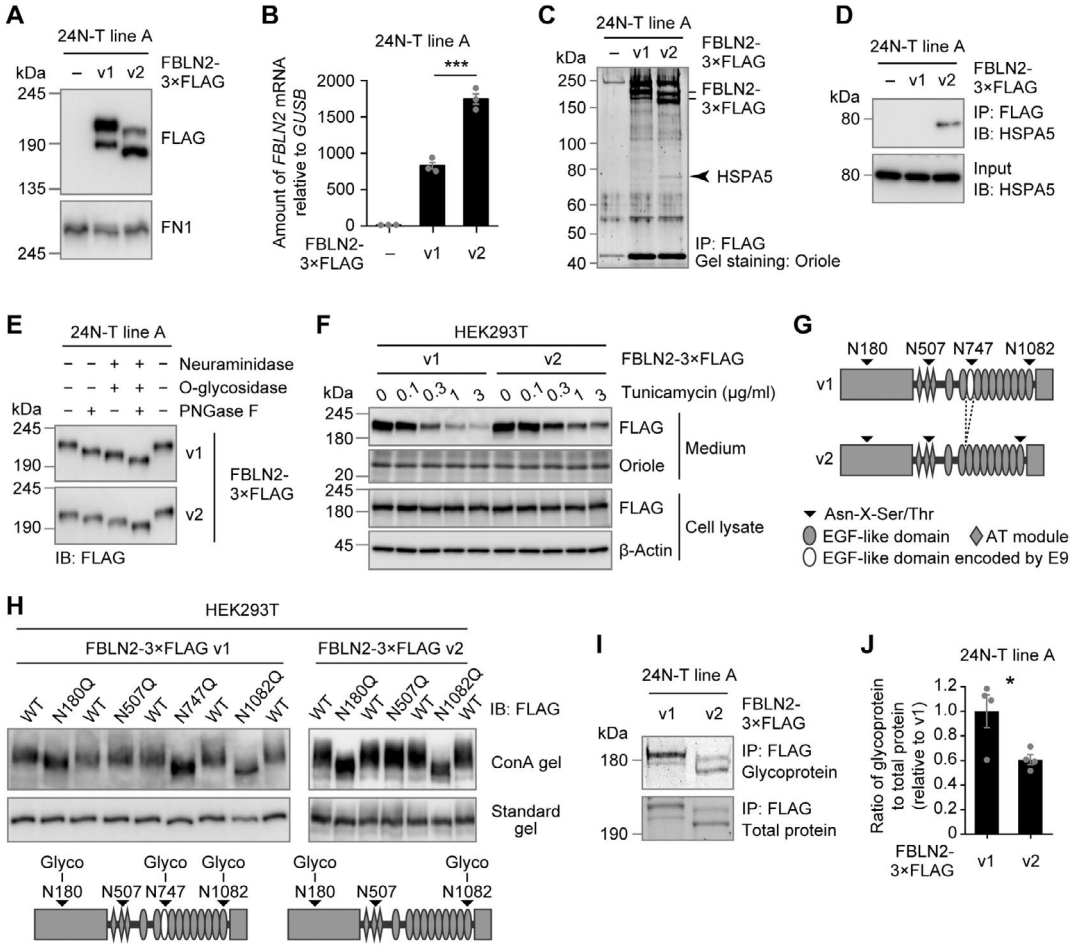

FIGURE 2 | Splicing of *FBLN2* exon 9 determines N-glycosylation of FBLN2 protein. (A, B) 24N-T fibroblasts infected (or not) with a recombinant lentivirus encoding FBLN2-3×FLAG v1 or v2 were subjected to immunoblot analysis with antibodies to FLAG (A) or to RT-qPCR analysis of *FBLN2* mRNA (B). FN1 expression was analyzed as a loading control in (A). Data in (B) are means ± SEM ($n = 3$ independent experiments). (C, D) 24N-T fibroblasts engineered as in (A) were subjected to immunoprecipitation (IP) with antibodies to FLAG, and the resulting precipitates were subjected to SDS-PAGE and staining with Oriole fluorescent dye (C) or to immunoblot analysis (IB) of HSPA5 (D). The arrowhead in (C) indicates the position of HSPA5 coprecipitated with FBLN2-3×FLAG v2. (E) FBLN2-3×FLAG v1 or v2 prepared from culture supernatants of 24N-T fibroblasts engineered as in (A) was treated (or not) with the indicated glycosidases and then subjected to immunoblot analysis of FLAG. (F) HEK293T cells expressing FBLN2-3×FLAG v1 or v2 were treated with various concentrations of tunicamycin, after which medium (culture supernatant) and cell lysate (cells attached to culture dish) were prepared and subjected to immunoblot analysis of FLAG. Oriole staining of the SDS-PAGE gel and immunoblot analysis of β-actin were performed as loading controls for medium and cell lysate fractions, respectively. (G) Schematic representation of human FBLN2 v1 and v2 proteins. Triangles indicate the positions of putative N-glycosylation sites. The positions of cbEGF-like domains and anaphylatoxin (AT) modules are also shown. (H) Immunoblot analysis of FLAG for HEK293T cells expressing WT or mutant versions of FBLN2-3×FLAG v1 or v2 (upper panel). Cell lysates were fractionated by SDS-PAGE in the presence (ConA gel) or absence (Standard gel) of concanavalin A. Schematic representations of N-glycosylation sites for v1 (bottom left) and v2 (bottom right) are also shown. (I) FBLN2-3×FLAG v1 or v2 immunoprecipitated from 24N-T fibroblasts engineered as in (A) was subjected to SDS-PAGE and stained for glycoproteins (upper) or total proteins (lower). The different mobility of protein size markers between glycoprotein gel (upper) and total protein gel (lower) is likely due to the use of distinct molecular weight standards, in which the 180 kDa marker band is glycosylated. (J) Quantification of signal intensity as in (I). Data are means ± SEM ($n = 4$ independent experiments). $^*p < 0.05$, $^{***}p < 0.001$ by Student's t test (B, J).

the lamina propria adjacent to the muscularis mucosae, as well as in blood vessels, where fibroblasts and vascular endothelial cells, respectively, are mainly found (Figure 1H). The FBLN2 protein was also detected in the muscularis mucosae itself, albeit at lower levels, but not in epithelial layers. Furthermore, RT-qPCR analysis of primary fibroblasts isolated from tumors or adjacent normal tissue of rectal or gastric cancer patients revealed that the abundance of *FBLN2* v2 mRNA was higher in the tumor-derived fibroblasts than in the normal tissue-derived fibroblasts (Figure 1I). These data thus demonstrate that the change in *FBLN2* splicing occurs in stromal cells, especially fibroblasts or blood endothelial cells of CRC tissue.

2.2 | Splicing of *FBLN2* Exon 9 Affects N-Glycosylation of FBLN2

Molecular difference between FBLN2 v1 and v2 is still not well documented. To pursue this issue, we generated immortalized fibroblasts (24N-T line A) that were derived from normal gastric

tissue of a gastric cancer patient and engineered to express 3×FLAG-tagged FBLN2 v1 or v2 (Figure 2A). FBLN2-3×FLAG in 24N-T fibroblasts was detected as two bands at positions corresponding to ~220 and ~190 kDa (Figure 2A). Cellular fractionation revealed that these bands corresponded to an extracellular mature form and an intracellular immature form of each variant, respectively (Figure S3), as predicted by a previous study (Sasaki et al. 1996). The FBLN2 v2 bands migrated faster than did the v1 bands because of the exclusion of exon 9 (Figure 2A). Of note, the intensity of the upper band was greater than that of the lower band for v1, whereas the opposite was the case for v2, suggesting that the maturation or secretion of v2 is less efficient than that of v1. Furthermore, RT-qPCR analysis unexpectedly revealed that the abundance of v2 mRNA was twice that of v1 mRNA (Figure 2B). Although the reason for this difference is unclear, these results suggested that the translation efficiency of *FBLN2* v2 mRNA or the stability of the v2 protein might be lower than those for v1.

To further characterize differences between FBLN2 v1 and v2, we explored variant-specific binding partners for FBLN2-3×FLAG. Whole cell lysates including both extracellular and intracellular proteins were subjected to immunoprecipitation with antibodies to FLAG, and Oriole gel staining of the precipitates revealed that v2 preferentially bound to a 75-kDa protein, which was identified as heat shock protein family A (Hsp70) member 5 (HSPA5) by liquid chromatography and tandem mass spectrometry (LC-MS/MS) (Figure 2C and Figure S4). We confirmed this finding by immunoprecipitation followed by immunoblot analysis (Figure 2D). HSPA5, also known as GRP78 or BiP, is a protein chaperone that recognizes misfolded proteins and assists their proper folding in the endoplasmic reticulum (ER) (Wang et al. 2017; Hetz et al. 2020). The preferential binding of v2 with HSPA5, together with our observation that v2 appeared to be secreted to a lesser extent compared with v1 (Figure 2A), suggested that the exclusion of *FBLN2* exon 9 might result in misfolding of the v2 protein and its binding to HSPA5 in the ER.

Protein glycosylation is one of the most prevalent posttranslational modifications that occur during protein synthesis in the ER and is crucial for the stability, folding, and secretion of ECM proteins (Schjoldager et al. 2020). FBLN2 undergoes both N-linked and O-linked glycosylation (Sicot et al. 2008), in which the glycan is attached to a nitrogen atom (N) of asparagine or to an oxygen atom (O) of serine or threonine. Indeed, treatment of extracellular FBLN2-3×FLAG secreted from 24N-T fibroblasts with peptide N-glycosidase F (PNGase F) or O-glycosidase, which cleave N-glycan or O-glycan, respectively, increased the electrophoretic mobility of the v1 and v2 bands (Figure 2E). Furthermore, treatment of HEK293T cells expressing FBLN2-3×FLAG v1 or v2 with tunicamycin, an inhibitor of N-glycosylation, attenuated the secretion of each variant in a concentration-dependent manner (Figure 2F), indicating that N-glycosylation is required for the efficient secretion of FBLN2. Of note, FBLN2 v1 possesses four consensus sequences (Asn-X-Ser/Thr) for N-glycosylation, among which N747 is located in the cbEGF-like domain encoded by exon 9 (Figure 2G), as reported previously (Pan et al. 1993; Sasaki et al. 1997).

To determine the N-glycosylation sites of FBLN2, we generated FBLN2-3×FLAG mutants in which potential N-glycosylation sites (Asn at amino acid positions 180, 507, 747, and 1082) were substituted with Gln (Figure 2G). HEK293T cells expressing the wild-type (WT) or mutant versions of FBLN2-3×FLAG were then subjected to SDS-polyacrylamide gel electrophoresis (PAGE) in the presence of concanavalin A, which binds to glycoproteins and thereby reduces their electrophoretic mobility (Popov et al. 2000). Immunoblot analysis with antibodies to FLAG revealed that the mobility of the v1 mutants N180Q, N747Q, or N1082Q was greater than that of the WT protein, whereas that of the N507Q mutant was similar to that of the WT protein, indicating that v1 is glycosylated at N180, N747, and N1082 (Figure 2H). Consistent with these results for v1, the mobility of the v2 mutants N180Q or N1082Q, but not that of N507Q, was greater than that of the WT protein, indicating that v2 is glycosylated at N180 and N1082 (Figure 2H). These data were further validated by analysis of FBLN2-3×FLAG mutants in which three of the four for v1 or two of the three for v2 potential N-glycosylation sites were simultaneously substituted with Gln (Figure S5). To evaluate the glycosylation level of FBLN2 v1 and v2, we subjected FBLN2-3×FLAG immunoprecipitates prepared from 24N-T cell lysates to SDS-PAGE followed by staining for glycoproteins or total proteins. We found that v2 was glycosylated to a lesser extent than was v1 (Figure 2I,J). Together, our results thus showed that FBLN2 v1 and v2 undergo N-glycosylation at different numbers of sites, three for v1 and two for v2 (Figure 2H).

2.3 | FBLN2 v2 Is More Unstable and Secreted to a Lesser Extent Than v1

The different N-glycosylation patterns between FBLN2 v1 and v2 prompted us to compare the stability and secretion efficiency of v1 and v2. To this end, we established 24N-T fibroblasts (line B) in which the abundance of FBLN2-3×FLAG v1 or v2 mRNAs was similar (Figure 3A). Immunoblot analysis revealed that the abundance of v2 protein was lower than that of v1 in both intracellular and extracellular fractions (Figure 3B,C), indicating that v2 might be less stable and secreted to a lesser extent than v1. Indeed, cycloheximide chase analysis showed that the intracellular immature form of v2 was degraded more rapidly than was that of v1 (Figure 3D,E). Furthermore, treatment of the cells with various concentrations of the proteasome inhibitor MG132 increased the abundance of the intracellular form of v2 to a greater extent than it did that of the intracellular form of v1 (Figure 3F,G), suggesting that v2 undergoes proteasomal degradation to a greater extent than does v1. Together, our findings thus indicated that FBLN2 v2, which is glycosylated at a lower level compared with v1, is less stable and secreted to a lesser extent than is v1.

2.4 | The ECM Environment of CRC Tissue Exhibits Low FBLN2 and High FN1 Abundance

Assuming that FBLN2 v2, which is the major splice variant expressed in CRC tumor tissue, is secreted to a lesser extent than v1 in fibroblast cultures, the abundance of extracellular FBLN2 could be lower in CRC tumor tissue than in corresponding normal tissue. To test this possibility, we examined the effect of *FBLN2* splicing on the expression of FBLN2 protein

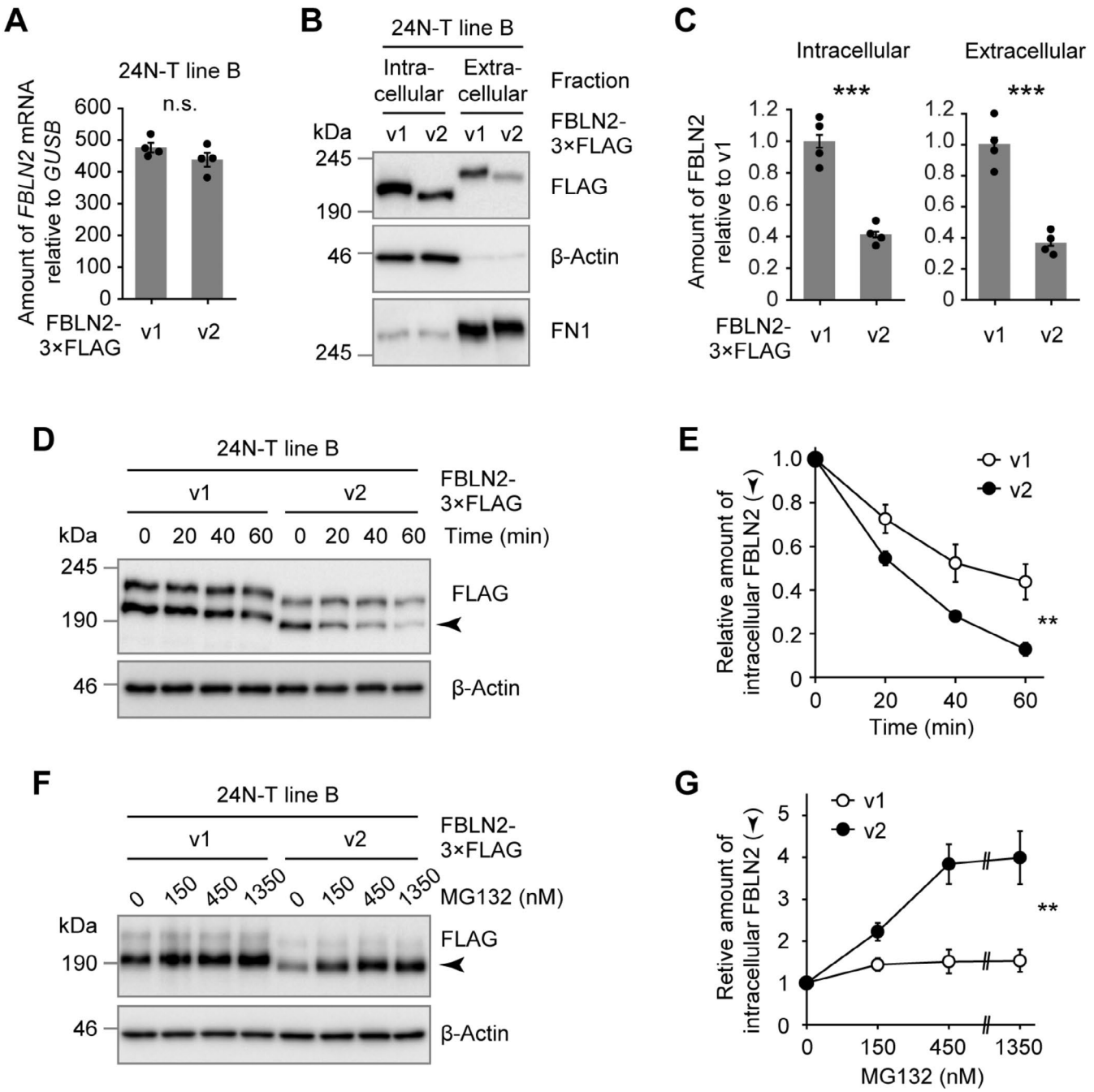

FIGURE 3 | FBLN2 v2 is less stable and secreted to a lesser extent compared with v1. (A–C) 24N-T fibroblasts infected with a recombinant retrovirus encoding FBLN2-3 × FLAG v1 or v2 were subjected to RT-qPCR analysis of *FBLN2* mRNA (A) or to cellular fractionation followed by immunoblot analysis of FLAG (B, C). Quantitative data are means ± SEM ($n = 4$ independent experiments). (D–G) 24N-T fibroblasts engineered as in (A) were incubated with cycloheximide (100 μg/mL) for the indicated times (D) or with various concentrations of MG132 for 6 h (F), after which cell lysates were subjected to immunoblot analysis of FLAG or β-actin (loading control). Arrowheads indicate the positions of the intracellular forms of FBLN2. Signal intensity for the intracellular forms of v1 and v2 was also determined (E, G), with the data presented as means ± SEM ($n = 4$ independent experiments). $^{**}p < 0.01$, $^{***}p < 0.001$, n.s. by Student's *t* test (A, C), by repeated measures ANOVA (E), or by two-way ANOVA (G).

in normal and primary tumor tissue of CRC patients. For immunoblot analysis, we tested three different FBLN2 antibodies that preferentially recognize the extracellular mature form of FBLN2 (ab96138 and HPA001934) or detect both the extracellular mature form and the intracellular immature form (sc-271263), hereafter referred to as total FBLN2 (Figure S3). Protein lysates prepared from normal or primary tumor tissue of CRC patients were then subjected to immunoblot analysis for total FBLN2 (sc-271263) or extracellular FBLN2 (ab96138) (Figure 4A). We adjusted for protein loading by staining for total proteins with Oriole fluorescent dye. Although immunoblot analysis of FBLN2-3 × FLAG in 24N-T fibroblasts showed two bands (Figure 2A), FBLN2 in CRC tissue lysates was detected as a single band with an apparent molecular size of ~220 kDa (Figure 4A). Consistent with our observation that the amount of *FBLN2* mRNA was reduced in tumor tissue

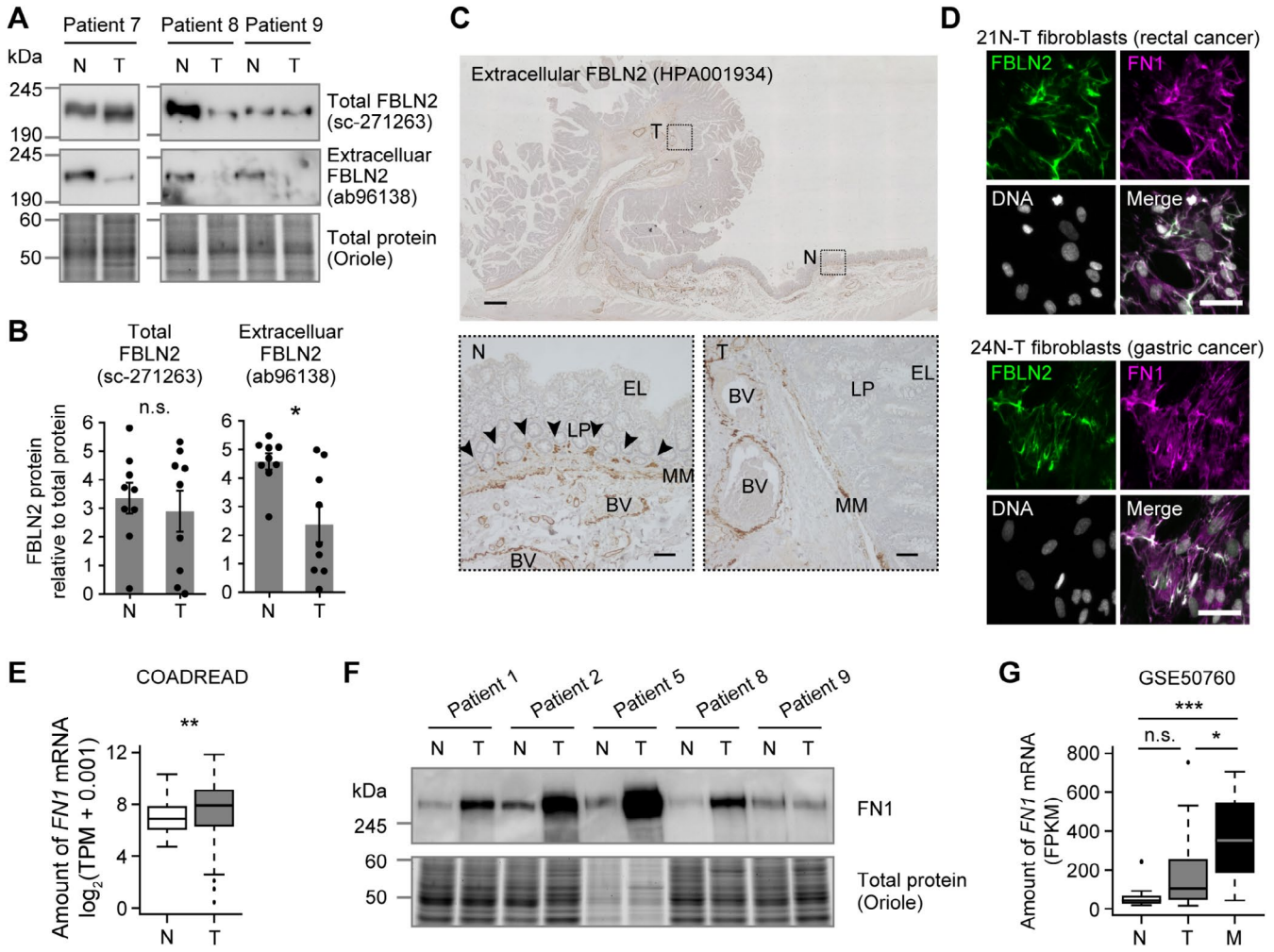

FIGURE 4 | The ECM environment of CRC tissue exhibits low FBLN2 and high FN1 abundance. (A) Lysates prepared from normal (N) or primary tumor (T) tissue of CRC patients were subjected to immunoblot analysis of FBLN2 with the indicated antibodies. The gel was also stained with Oriole fluorescent dye to allow adjustment for protein loading. (B) Quantification of signal intensity as in (A). Data are means ± SEM ($n = 9$ patients). (C) Representative immunohistochemical staining of extracellular FBLN2 (HPA001934) in a section containing primary tumor (T) and adjacent normal (N) tissue isolated from a CRC patient. The boxed regions in the upper image are shown at higher magnification in the lower images. FBLN2 signals in the lamina propria (LP) are indicated by arrowheads in the lower left image. BV, blood vessel; EL, epithelial layer; MM, muscularis mucosae. Scale bars, 1 mm (upper) and 100 μm (lower). (D) Representative immunofluorescence analysis of FBLN2 and FN1 in 21N-T (upper) or 24N-T (lower) fibroblasts isolated from rectal cancer or gastric cancer patients, respectively. DNA was stained with 4′,6-diamidino-2-phenylindole (DAPI). Scale bars, 50 μm. (E) Box plots for *FN1* mRNA level based on transcripts per million (TPM) in normal (N) and primary tumor (T) tissue for COADREAD in TCGA. (F) Immunoblot analysis of FN1 in lysates prepared from normal (N) and primary tumor (T) tissue of CRC patients. The gel was stained for total proteins with Oriole fluorescent dye. (G) Box plots for *FN1* mRNA level based on fragments per kilobase of exon per million mapped reads (FPKM) in normal (N), primary CRC tumor (T), and metastatic liver tumor (M) tissue determined by RNA-seq analysis (GSE50760) as in Figure 1D. $^*p < 0.05$, $^{**}p < 0.01$, $^{***}p < 0.001$, n.s. by the paired *t* test (B), Wilcoxon rank sum test (E) or by one-way ANOVA followed by Tukey's post hoc test (G).

of COAD and READ relative to corresponding normal tissue (Figure S2), we found that the abundance of total FBLN2 protein was reduced in tumor tissue relative to normal tissue of some CRC patients, including patient 8 (Figure 4A and Figure S6). However, no significant difference was observed in the average total FBLN2 protein level between normal and tumor tissue of all the patients (Figure 4B), likely because of the high variability in such expression levels and the limited number of samples. Of note, however, the amount of extracellular FBLN2 was markedly reduced in tumor tissue relative to normal tissue, even for patients (such as patients 7 and 9) who showed similar levels of total FBLN2 in normal and tumor samples (Figure 4A and Figure S6). The average abundance of extracellular FBLN2 was thus significantly lower in tumor tissue than in normal tissue (Figure 4B).

To further analyze the effect of *FBLN2* splicing on FBLN2 protein expression, we performed immunohistochemical analysis of CRC and adjacent normal tissue for extracellular FBLN2 (HPA001964). The FBLN2 signal was evident in the lamina propria adjacent to the muscularis mucosae in normal tissue, whereas it was attenuated in the lamina propria at the boundary between normal and tumor tissue and was not detected at all in that of tumor tissue (Figure 4C and Figure S7). FBLN2 expression in blood vessels and

the muscularis mucosae appeared similar between normal and tumor tissue. Together, these results thus suggested that the exclusion of *FBLN2* exon 9 results in a reduction in the abundance of extracellular FBLN2 in the lamina propria of CRC tissue.

FBLN2 binds to various ECM proteins, the expression of which could be altered in tumor tissue compared with normal tissue. We then focused on and examined FN1 expression, given that FBLN2 binds to FN1 in vitro and colocalizes with FN1 in the ECM of cultured human foreskin fibroblasts (Sasaki et al. 1995, 1996). Indeed, we found that FBLN2 was also colocalized with FN1 in the ECM of fibroblast cultures derived from corresponding normal tissue of patients with rectal or gastric cancer (Figure 4D). The expression of FN1 was previously shown to be increased in tumor tissue of gastrointestinal cancers including CRC, gastric cancer, and esophageal squamous cell carcinoma compared with corresponding normal tissue (Yi et al. 2016; Cai et al. 2018; Xiao et al. 2018; Sun et al. 2020; Ye et al. 2020). Consistent with these findings, our analysis of TCGA RNA-seq data showed that the abundance of *FN1* mRNA was increased in tumor tissue of COAD and READ (COADREAD) relative to normal tissue (Figure 4E). Immunoblot analysis of normal and tumor tissue isolated from CRC patients revealed that FN1 expression was also increased at the protein level in tumor tissue (Figure 4F). Furthermore, analysis of the GSE50760 data set showed that *FN1* expression was increased to an even greater extent in metastatic liver tumors than in primary CRC tumors relative to normal tissue (Figure 4G). This change in *FN1* expression was opposite to that apparent for the splicing-in of *FBLN2* exon 9 in the same samples (Figure 1D). These results indicated that the ECM of tumor tissue is characterized by a decreased FBLN2 content but increased FN1 content compared with that of normal tissue in CRC patients.

2.5 | FBLN2 Suppresses the Adhesion and Migration of CRC Cells

We finally explored whether the elevated FN1 and reduced FBLN2 abundance in the ECM of tumor tissue might contribute to the progression of CRC. Given that both *FN1* expression and *FBLN2* splicing showed larger changes in metastatic liver tumors than in primary tumors, we examined the role of FN1 and FBLN2 in the regulation of cell migration in the context of ECM. To test the effects of extracellular FN1 and FBLN2 on the migration of CRC cells in vitro, we performed a transwell migration assay for quantification of the migration of HCT 116 cells (human CRC cell line) through a microporous membrane coated with FN1 or FBLN2 protein (Bouchalova and Bouchal 2022). Given that the major FBLN2 variant in tumor tissue is v2, we examined the effect of commercially available recombinant FBLN2 v2. Although FN1 promoted the migration of HCT 116 cells compared with the noncoated control, as expected from previous findings (Xia et al. 2017; Cai et al. 2018; Xiao et al. 2018), FBLN2 v2 almost completely suppressed it (Figure 5A,B). To investigate the effect of FBLN2 v2 on FN1-induced cell migration, we coated the membrane with a mixture of a fixed concentration (20 μg/mL) of FN1 and various concentrations (0–20 μg/mL) of FBLN2 v2 or of bovine serum albumin (BSA) as a control. FBLN2 v2, but not BSA, suppressed FN1-induced migration of HCT 116 cells in a concentration-dependent manner (Figure 5C,D).

We then examined whether the ability of FBLN2 v2 to inhibit cell migration is shared by FBLN2 v1. We purified FBLN2 v2 and FBLN2 v1 from immortalized fibroblasts (24N-T line A) engineered to express 3 × FLAG-tagged FBLN2 v1 or v2 (Figure 2A). Each FBLN2-3 × FLAG variant was thus prepared from culture supernatants of these cells by immunoprecipitation with antibodies to FLAG (Figure S8A). Purified FBLN2 v1 suppressed the FN1-induced migration of HCT 116 cells to a similar extent as did purified FBLN2 v2 (Figure S8B,C), showing that the two variants did not differ substantially in their ability to inhibit such cell migration.

FN1 in ECM binds to cell surface integrins to promote cell migration (Efthymiou et al. 2020; Spada et al. 2021). Given that FBLN2 binds to FN1 in vitro and colocalizes with FN1 in fibroblast cultures (Figure 4D) (Sasaki et al. 1995, 1996), we examined whether FBLN2 suppresses FN1-induced cell migration by interrupting the interaction between FN1 and CRC cells. To test this notion, we performed a cell adhesion assay in which HCT 116 cells adhere to the surface of a low-attachment cell culture dish coated with FN1 or FBLN2 v2. As expected, coating with FN1 increased the adhesion of HCT 116 cells to the dish in a concentration-dependent manner (Figure S9). However, in the presence of a fixed amount of FN1, FBLN2 v2 (but not BSA) attenuated cell adhesion in a concentration-dependent manner (Figure 5E,F). Together, these results showed that FBLN2 v2 suppresses CRC cell adhesion to and migration on FN1 in vitro. An ECM characterized by reduced FBLN2 and elevated FN1 levels might therefore promote tumor cell metastasis in CRC.

3 | Discussion

We found that exon 9 of *FBLN2* is excluded from mRNA in tumor tissue across various types of solid cancer—in particular, in gastrointestinal cancers including CRC. *FBLN2* mRNA was detected predominantly in fibroblasts and vascular endothelial cells in CRC tissue, suggesting that this splicing change takes place in either or both of these cell types. The exclusion of exon 9 results in the loss of a single N-glycosylation site in the excluded cbEGF-like domain, which in turn leads to a reduction in the stability and the extent of secretion of the FBLN2 v2 protein. The tumor ECM is thus characterized by a low abundance of FBLN2 and a high FN1 content, a composition that promotes the migration of CRC cells (Figure 5G). The alternative splicing of *FBLN2* exon 9 might therefore contribute to the invasion and metastasis of cancer cells through remodeling of the tumor ECM.

Dysregulation of glycosylation is a hallmark of cancer. Altered expression of glycosylation enzymes is thus common in cancer and results in distinct combinations and extents of protein glycosylation (Pinho and Reis 2015). Changes in glycosylation sites of substrate proteins have also been identified in the context of cancer. Gene mutations that affect glycosylation motifs can thus affect glycosylation (Fan et al. 2018), whereas changes in transcript splicing can lead to the gain or loss of glycosylation sites (Wasser et al. 2014; Huang et al. 2019). Our study now provides an example of the latter mechanism that was found to have consequences for cancer cell migration.

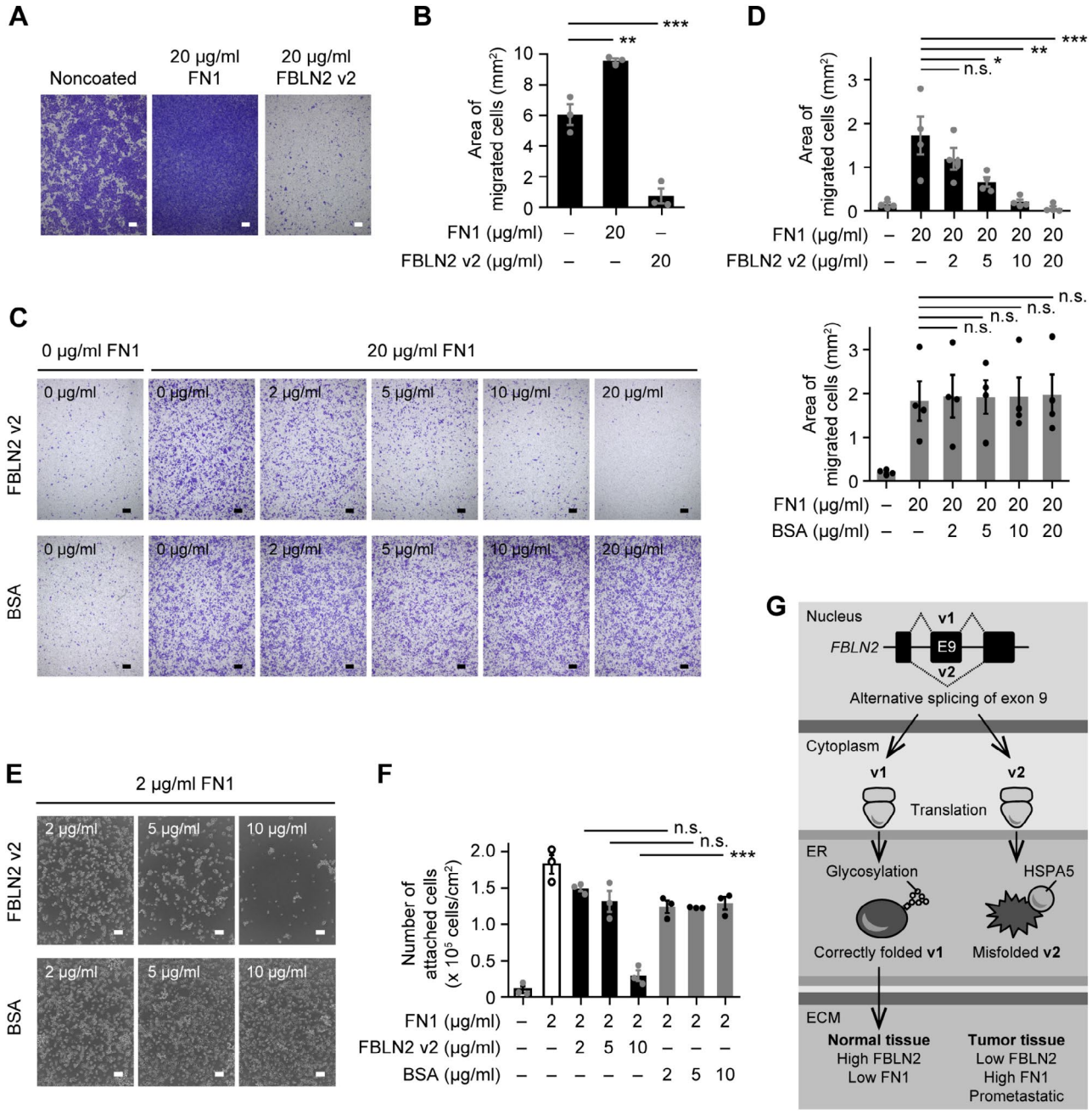

FIGURE 5 | FBLN2 suppresses the adhesion and migration of CRC cells. (A) Representative results for a transwell migration assay in which HCT 116 cells were seeded on a transwell insert coated (or not) with FN1 (20 μg/mL) or FBLN2 v2 (20 μg/mL) and were then allowed to migrate for 48 h. (B) Quantification of the area of migrated cells as in (A). Data are means ± SEM ($n = 3$ independent experiments). (C) Representative results for a transwell migration assay in which HCT 116 cells were seeded on a transwell insert coated (or not) with FN1 (20 μg/mL) and various concentrations of FBLN2 v2 or BSA and were then allowed to migrate for 24 h. (D) Quantification of the area of migrated cells as in (C). Data are means ± SEM ($n = 4$ independent experiments). (E) Representative results for a cell adhesion assay in which HCT 116 cells were seeded in low-attachment dishes coated (or not) with FN1 (2 μg/mL) and various concentrations of FBLN2 v2 or BSA. (F) Quantification of attached cells as in (E). (G) Model for the role of alternative splicing of *FBLN2* exon 9 in the remodeling of ECM. Data are means ± SEM ($n = 3$ independent experiments). *$p < 0.05$, **$p < 0.01$, ***$p < 0.001$, n.s. by one-way ANOVA followed by Tukey's post hoc test (B, D, F). Scale bars, 200 μm (A, C) and 100 μm (E).

Changes in N-glycosylation of ECM proteins can influence protein stability by inducing misfolding during protein synthesis in the ER as well as protein–protein interaction by altering protein structure (Lee et al. 2015; Xu and Ng 2015; Peixoto et al. 2019). We found that HSPA5 is preferentially bound to the v2 isoform of FBLN2, suggesting that the loss of the single glycosylation site in the excluded cbEGF-like domain induces misfolding of FBLN2. Unfolded proteins are recognized by ER chaperones such as HSPA5, leading to either restoration of correct folding or degradation of the unstructured proteins. Of note, FBLN3, another member of the fibulin family, was found to be destabilized as a result of defective glycosylation of a cbEGF-like domain that resulted in increased binding to ER chaperones (Hulleman and Kelly 2015; Woodard et al. 2021). The loss of glycosylation

of cbEGF-like domains may therefore give rise to protein misfolding and a consequent downregulation of the abundance and secretion of fibulin proteins. We did not detect a difference in the abilities of the v1 and v2 isoforms of FBLN2 to inhibit FN1-mediated cell migration, suggesting that the difference in N-glycosylation between the two isoforms does not substantially affect the association between FBLN2 and FN1. ECM remodeling can be achieved by changes in either the expression or activity of ECM proteins. Given that FBLN2 has been found to interact with many ECM proteins (Pan et al. 1993; Sasaki et al. 1995, 1997; Timpl et al. 2003), it will be of interest to investigate whether the reduced level of glycosylation of FBLN2 v2 affects its interaction with binding partners other than FN1.

The mechanism underlying regulation of the splicing of *FBLN2* exon 9 in cancer tissue remains unknown. Splicing of exon 9 of *Fbln2* undergoes a change in mouse cardiomyocytes during postnatal heart development (Giudice et al. 2014; Hinkle et al. 2022). Increased blood flow also increases the inclusion of *Fbln2* exon 9 in an RBFOX2-dependent manner in mouse arterial endothelium (Murphy et al. 2018). Furthermore, human cytomegalovirus infection increases the expression of CPEB1, which in turn results in the exclusion of *FBLN2* exon 9, in human foreskin fibroblasts and neural progenitor cells (Batra et al. 2016). Both cell-intrinsic and extrinsic mechanisms might therefore contribute to the regulation of *FBLN2* splicing. In addition to RBFOX2 and CPEB1, other RNA binding proteins—including PTBP1 (Hinkle et al. 2022), QKI (Hinkle et al. 2022), MBNL1 (Giudice et al. 2014), and CELF1 (Giudice et al. 2014)—have been shown to regulate the inclusion of *FBLN2* exon 9. The identification of such proteins as well as environmental cues that promote the exclusion of *FBLN2* exon 9 in cancer tissue should provide not only insight into the mechanism underlying the generation of a prometastatic tumor ECM but also a basis for the development of new anticancer agents.

Our study has several limitations. First, although we identified fibroblasts and vascular endothelial cells as the most likely cell types in which the splicing pattern of *FBLN2* exon 9 is altered in tumor tissue, our data do not exclude the possible involvement of other cell types. Second, although we found that the reduced glycosylation level of FBLN2 v2 contributes to a reduced extent of FBLN2 secretion and the generation of a prometastatic ECM environment using in vitro models, the roles of *FBLN2* splicing and resultant production of FBLN2 v2 in the invasion and metastasis of cancer cells in vivo remain to be clarified.

In the early stages of tumor invasion, CRC cells invade the lamina propria and muscularis mucosae, and we found that extracellular FBLN2 was present in the lamina propria of normal tissue but not in that of tumor tissue. We also found that extracellular FBLN2 v2 suppressed the adhesion of CRC cells to FN1 as well as their FN1-dependent migration in vitro. These results suggest that the loss of extracellular FBLN2 in the tumor ECM, which results from the exclusion of exon 9 of the gene, might promote the migration and invasion of CRC cells at the lamina propria and muscularis mucosae. Consistent with this notion, ectopic expression of FBLN2 was previously shown to attenuate the migration and invasion of nasopharyngeal cancer cells (Law et al. 2012), non-small cell lung cancer cells (Ma et al. 2021), and breast cancer cells (Yi et al. 2007; Zhang, Duan, et al. 2020). Conversely, however, knockdown of FBLN2 was also shown to suppress the migration, invasion, and metastatic capacity of lung adenocarcinoma cells in mice (Baird et al. 2013). In addition, FBLN2 together with NID1 increased the migration of CRC cells in cell culture (Vaes et al. 2021). Further studies to determine the role of FBLN2 in the regulation of invasion and metastasis of CRC cells in vivo are therefore warranted. The establishment of mice that express FBLN2 v1 or v2 exclusively may shed additional light on the functional relevance of *FBLN2* splicing in cancer.

4 | Experimental Procedures

4.1 | Analysis of RNA-Seq Data

The percent spliced-in (PSI) values for *FBLN2* exon 9 in TCGA samples were downloaded from the website (https://bioinformatics.mdanderson.org/TCGASpliceSeq/index.jsp) of the TCGASpliceSeq database (Ryan et al. 2016). For analysis of *FBLN2* and *FN1* expression in TCGA samples, gene expression data were downloaded from the Xena website (https://xena.ucsc.edu) of the University of California at Santa Cruz (Goldman et al. 2020). The scRNA-seq data for Human Colon Cancer Atlas (c295, GSE178341) were downloaded from the website (https://singlecell.broadinstitute.org/single_cell) of the Single Cell Portal (Pelka et al. 2021).

For analysis of the RNA-seq data set GSE50760, the fastq files were obtained from the website (https://www.ncbi.nlm.nih.gov/geo) of the National Center for Biotechnology Information (NCBI) (Barrett et al. 2013; Kim et al. 2014). This data set includes data for normal (N), primary tumor (T), and metastatic liver tumor (M) tissue isolated from 18 CRC patients (total of 54 samples). The inclusion or exclusion of *FBLN2* exon 9 was analyzed with the use of vast-tools software (Irimia et al. 2014). The PSI value was calculated according to the equation: $\mathrm{PSI} = 100 \times (\text{inclusion level}) / (\text{inclusion level} + \text{exclusion level})$. Cufflinks (ver. 2.0.10) was applied to estimate gene expression level on the basis of fragments per kilobase of transcript per million mapped reads (FPKM) (Trapnell et al. 2010).

4.2 | Surgical Specimens

Colorectal tissue specimens were obtained from nine CRC patients who underwent surgical resection of the primary tumor at Tohoku University Hospital. This aspect of the study was approved by the Institutional Review Board of Tohoku University Graduate School of Medicine (approval nos. 2016-1-177 and 2022-1-1056), and the patients provided written informed consent.

4.3 | Cell Culture and Transfection

HCT 116 (RRID: CVCL_0291) and HEK293T (RRID: CVCL_0063) cells were obtained from American Type Culture Collection and were authenticated by short tandem repeat (STR) profiling. Primary fibroblasts were established from normal or tumor tissue isolated from rectal or gastric cancer patients as described previously (Aizawa et al. 2019).

The fibroblasts isolated from the normal tissue of rectal or gastric cancer patients were immortalized by the introduction of telomerase reverse transcriptase (TERT) to generate 21N-T and 24N-T fibroblasts, respectively. HCT 116 cells were cultured in McCoy's 5A medium (Thermo Fisher Scientific), and HEK293T cells and fibroblasts in Dulbecco's modified Eagle's medium (DMEM, Nacalai Tesque), with each medium being supplemented with 10% heat-inactivated fetal bovine serum (FBS, Thermo Fisher Scientific). All cells were maintained under a humidified atmosphere of 5% CO_2 at 37°C, and all experiments were performed with mycoplasma-free cells. The lentiviral vector CSII-EF-MCS-IRES-Puro and retroviral vector pMXpuro were used to generate 24N-T fibroblasts (lines A and B, respectively) that express human FBLN2 tagged with the 3×FLAG epitope at the COOH-terminus (FBLN2-3×FLAG). The 24N-T fibroblasts were thus infected with recombinant lentiviruses or retroviruses encoding FBLN2-3×FLAG v1 or v2, and the infected cells were subjected to selection for 3 days in medium containing puromycin (Sigma-Aldrich) at 5 μg/mL.

4.4 | RT-qPCR Analysis

Total RNA was isolated from tumor tissue or cultured cells with the use of an SV Total RNA Isolation System (Promega) and was subjected to RT with the use of a PrimeScript RT Reagent Kit (Takara Bio). Quantitative PCR (qPCR) analysis was performed with Fast SYBR Green Master Mix (Thermo Fisher Scientific) and a StepOnePlus Real-Time PCR System (Thermo Fisher Scientific). The total mRNA abundance for *FBLN2* (including both v1 and v2) was normalized by the amount of glucuronidase-β (*GUSB*) mRNA. The abundance of *FBLN2* v1 and v2 mRNAs was determined from standard curves obtained with corresponding cDNAs. Primer sequences and qPCR conditions are provided in Table S1.

4.5 | Immunostaining

For immunohistochemistry of tumor tissue, paraffin-embedded sections were stained with primary antibodies to FBLN2 (HPA001934, Sigma-Aldrich). Immune complexes were detected with peroxidase-labeled secondary antibodies and 3,3′-diaminobenzidine (Histofine SAB-PO(M) Kit, Nichirei Bioscience), and the sections were counterstained with hematoxylin. For immunofluorescence analysis of 21N-T and 24N-T fibroblasts, the cells were fixed with 3.7% formaldehyde and stained with primary antibodies to FBLN2 (HPA001934, Sigma-Aldrich) or to FN1 (MS-167-P0, NeoMarkers). Immune complexes were detected with Alexa Fluor 488- or Alexa Fluor 594-labeled secondary antibodies (Thermo Fisher Scientific), and the cells were counterstained with DAPI. Samples were observed with a BZ-9000 microscope (Keyence).

4.6 | Immunoblot Analysis and Oriole Gel Staining

Tumor tissue or cultured cells were lysed with Cell Lysis Buffer consisting of 50 mM Tris-HCl (pH 7.4), 300 mM NaCl, 0.5% Triton X-100, 400 μM sodium orthovanadate, 400 μM EDTA, 10 mM NaF, 10 mM sodium pyrophosphate, aprotinin (2 μg/mL), leupeptin (2 μg/mL), and 1 mM phenylmethylsulfonyl fluoride (PMSF). Lysates were centrifuged at 20,000*g* for 10 min at 4°C, and the resulting supernatants were subjected to SDS-PAGE. For immunoblot analysis, the separated proteins were transferred to a polyvinylidene difluoride membrane (Millipore), which was then probed with primary antibodies to FBLN2 (sc-271263, Santa Cruz; ab96138, Abcam; or HPA001934, Sigma-Aldrich), to FN1 (MS-167-P0, NeoMarkers), to FLAG (F3165, Sigma-Aldrich), to HSPA5 (66574-1-Ig, ProteinTech), or to β-actin (3700, Cell Signaling Technology). Immune complexes were detected with horseradish peroxidase-conjugated secondary antibodies (Promega) and Super Signal West Substrate (Thermo Fisher Scientific). For visualization of total proteins, the SDS-PAGE gel was stained with Oriole Fluorescent Gel Stain (Bio-Rad). The chemiluminescence and fluorescence signals were detected with the use of a digital imaging system (ChemiDoc Touch, Bio-Rad).

4.7 | Immunoprecipitation

Cells were lysed with Immunoprecipitation Lysis Buffer consisting of 50 mM Tris-HCl (pH 7.4), 150 mM NaCl, 0.5% Triton X-100, 400 μM sodium orthovanadate, 400 μM EDTA, 10 mM NaF, 10 mM sodium pyrophosphate, aprotinin (2 μg/mL), leupeptin (2 μg/mL), and 1 mM PMSF. The lysate was centrifuged at 20,000*g* for 10 min at 4°C, and the resulting supernatant (~2 mg of protein) was incubated for 1 h at 4°C with Dynabead Protein G (Thermo Fisher Scientific)-conjugated antibodies to FLAG (8 μg; F3165, Sigma-Aldrich). The immunoprecipitates were washed twice with Immunoprecipitation Lysis Buffer and subjected to elution with 3×FLAG peptide (5 mg/mL, Sigma-Aldrich).

4.8 | LC-MS/MS Analysis

Immunoprecipitates prepared with antibodies to FLAG were fractionated by SDS-PAGE and stained with silver (Sigma-Aldrich). The stained gel was sliced into nine pieces per lane, and the proteins in these slices were subjected to in-gel digestion with trypsin (Promega). The resulting peptides were applied to a nanoflow LC system (Advance UHPLC, Bruker) equipped with an in-house pulled fused silica capillary (0.1 mm×10 cm) packed with a 3-μm C18 L-column (CERI). Eluted peptides were sprayed directly into an LTQ Orbitrap Velos Pro mass spectrometer (Thermo Fisher Scientific). LC-MS/MS analysis was performed with three biological replicates.

4.9 | Analysis of FBLN2 Glycosylation

Culture supernatants of 24N-T line A fibroblasts expressing FBLN2-3×FLAG v1 or v2 were passed through a 0.45-μm syringe filter and treated with PNGase F (New England Biolabs) or O-glycosidase (New England Biolabs) together with neuraminidase (New England Biolabs) for 2 h at 37°C before immunoblot analysis with antibodies to FLAG. For analysis of the effects of tunicamycin, HEK293T cells transfected with CSII-EF-MCS-IRES-Puro vector encoding FBLN2-3×FLAG v1 or v2 were treated with tunicamycin (Cayman Chemical)

for 2 days, after which culture supernatant (medium) and total cell lysates (cell lysate) were prepared. The culture supernatant was passed through a 0.45-μm syringe filter. The samples were subjected to immunoblot analysis and Oriole gel staining. For the identification of N-glycosylation sites of FBLN2, lysates of HEK293T cells transfected with vectors encoding WT or mutant forms of FBLN2-3×FLAG v1 or v2 were fractionated by SDS-PAGE on a gel containing concanavalin A (7–10 mg/mL; L7647, Sigma-Aldrich) as described previously (Popov et al. 2000) and then subjected to immunoblot analysis of FLAG. For analysis of glycosylation level, FBLN2-3×FLAG v1 or v2 was immunoprecipitated from lysates of 24N-T line A fibroblasts, subjected to SDS-PAGE, and stained for glycoproteins with the use of a Pro-Q Emerald 488 Glycoprotein Gel and Blot Stain Kit (Thermo Fisher Scientific) or for total proteins with Oriole fluorescent dye.

4.10 | Cellular Fractionation of Fibroblasts

Culture supernatant of 24N-T line A fibroblasts expressing FBLN2-3×FLAG v1 or v2 was passed through a 0.45-μm syringe filter, and the filtrate was analyzed as an extracellular fraction. The remaining cells were treated with 0.25% trypsin (Nacalai Tesque) for 15 min at 37°C under 5% CO_2 to degrade cell surface proteins, isolated by centrifugation at 200 *g* for 2 min at 4°C, and lysed with Cell Lysis Buffer. The lysate was centrifuged at 20,000 *g* for 10 min at 4°C, and the resulting supernatant was analyzed as an intracellular fraction. Both extracellular and intracellular fractions were subjected to immunoblot analysis.

4.11 | Cycloheximide Chase Assay and MG132 Treatment

24N-T line B fibroblasts expressing FBLN2-3×FLAG v1 or v2 were treated with cycloheximide (100 μg/mL, Sigma-Aldrich) for up to 60 min or with MG132 (Peptide Institute) for 6 h at 37°C and under 5% CO_2. The MG132-treated cells were washed with cold PBS three times before cell lysis to prevent the contamination of dead cells. The treated cells were subjected to immunoblot analysis.

4.12 | Transwell Migration Assay and Cell Adhesion Assay

For the transwell migration assay, the lower side of the filter membrane (diameter of 6.5 mm, pore size of 8 μm; 3422, Corning) was treated with FN1 (F0895, Sigma-Aldrich), recombinant FBLN2 v2 (9559-FB-050, R&D Systems), or BSA (017-23294, Fujifilm Wako) for 10 min and then allowed to dry for 30 min. HCT 116 cells were suspended in serum-free McCoy's 5A medium, seeded at a density of 5×10^4 per membrane, and allowed to migrate for 24 or 48 h at 37°C and under 5% CO_2. McCoy's 5A medium supplemented with 10% FBS was added to the lower chamber as the chemoattractant. The cells were fixed and stained with methanol containing 0.3% crystal violet (Fujifilm Wako) for 20 min and then washed with phosphate-buffered saline. After removal of nonmigrated cells on the upper side of the membrane with a cotton swab, the membrane was observed with a BZ-9000 microscope (Keyence). The area of migrated cells was determined with ImageJ software version 1.52a (Schneider et al. 2012).

For the migration assay shown in Figure S8B, the lower side of the filter membrane was treated with FN1(F0895, Sigma-Aldrich) and with FBLN2 v1 or FBLN2 v2 purified from culture supernatants of engineered 24N-T fibroblasts expressing FBLN2-3×FLAG v1 or v2. The culture supernatants collected from cells maintained for 3–4 days from an initial confluence of 80% in one 150-mm dish and one 100-mm dish were passed through a 0.45-μm syringe filter (Minisart 17598-K, Sartorius), and the filtrate (~35 mL) was incubated overnight at 4°C with Dynabead Protein G (Thermo Fisher Scientific)-conjugated antibodies to FLAG (8 μg; F3165, Sigma-Aldrich) in 10 mL of RIPA Buffer consisting of 50 mM Tris-HCl (pH 7.4), 150 mM NaCl, 1% Nonidet P-40, 0.5% sodium deoxycholate, 0.1% SDS, 400 μM sodium orthovanadate, 400 μM EDTA, 10 mM NaF, 10 mM sodium pyrophosphate, aprotinin (2 μg/mL), leupeptin (2 μg/mL), and 1 mM PMSF. The immunoprecipitates were washed twice with RIPA Buffer and subjected to elution with 200 μL of 3×FLAG peptide (5 mg/mL, Sigma-Aldrich) in Elution Buffer consisting of 10 mM HEPES-NaOH (pH 7.3), 150 mM NaCl, and 0.05% Triton X-100. The eluted material was verified by SDS-PAGE followed by Oriole gel staining and immunoblot analysis before use for membrane coating.

For the cell adhesion assay, 200 μL of FN1 (F0895, Sigma-Aldrich), recombinant FBLN2 v2 (9559-FB-050, R&D Systems), or BSA (017-23294, Fujifilm Wako) were applied to the surface of a low-attachment dish (diameter of 60 mm; MS-1160R, Sumitomo Bakelite). The solution was covered with a nylon filter with a pore size of 85 μm (3 by 3 cm, Nippon Rikagaku Kikai) to keep the solution within a 3 by 3 cm area and incubated for 24 h at 37°C and under 5% CO_2. The solution was then removed, and the dish was allowed to dry for 1 h. HCT 116 cells were plated at a density of 3×10^6 cells per dish and cultured for 8 h, after which the attached cells in the coated area were observed with a BZ-9000 microscope (Keyence) and their number was determined with the use of a TC20 automated cell counter (Bio-Rad).

4.13 | Statistical Analysis

Unless indicated otherwise, quantitative data are presented as means ± SEM for the indicated number (*n*) of biological replicates, and they were subjected to statistical analysis with R software version 4.0.3 or Excel for Microsoft 365. A p value of <0.05 was considered statistically significant.

Author Contributions

Ryo Funayama: conceptualization, investigation, funding acquisition, writing – original draft, writing – review and editing. **Yujue Wang:** conceptualization, investigation. **Masaki Hosogane:** conceptualization, investigation, funding acquisition, writing – original draft, writing – review and editing. **Wei-Chen Kao:** conceptualization, investigation. **Shingo Toyama:** conceptualization, investigation. **Masahiro Ohira:** investigation. **Masaki Matsumoto:** investigation. **Takashi Aizawa:** resources. **Minoru Kobayashi:** supervision, writing – review and editing, resources. **Hideaki Karasawa:** supervision, resources. **Shinobu Ohnuma:** supervision, resources, writing – review and editing.

Keiichi I. Nakayama: resources, supervision, writing – review and editing. **Michiaki Unno:** supervision, resources, writing – review and editing. **Keiko Nakayama:** conceptualization, supervision, funding acquisition, writing – original draft, writing – review and editing.

Acknowledgments

We thank all the patients and family members for their participation in this study. The results presented here are based in part on data generated by the TCGA Research Network (https://www.cancer.gov/tcga). We also thank H. Miyoshi for providing the lentiviral vector CSII-EF-MCS-IRES-Puro; Y. Nagasawa, K. Kuroda, and M. Kikuchi for technical assistance; T. Konishi for help with the preparation of the manuscript; other laboratory members for discussion; and the Biomedical Research Core of Tohoku University Graduate School of Medicine for technical support.

Ethics Statement

This study was approved by the Institutional Review Board of Tohoku University Graduate School of Medicine (approval nos. 2016-1-177 and 2022-1-1056), and the patients provided written informed consent.

Conflicts of Interest

K.I.N. is an Editorial Board Member of Genes to Cells. The other authors declare no conflicts of interest.

Data Availability Statement

The data that support the findings of this study are openly available in the TCGASpliceSeq database at https://bioinformatics.mdanderson.org/TCGASpliceSeq/index.jsp (Ryan et al. 2016), the Xena website at https://xena.ucsc.edu (Goldman et al. 2020), the SingleCell Portal (Human Colon Cancer Atlas, c295, GSE178341) at https://singlecell.broadinstitute.org/single_cell (Pelka et al. 2021), and the NCBI (GSE50760) at https://www.ncbi.nlm.nih.gov/geo (Barrett et al. 2013; Kim et al. 2014).

References

Aizawa, T., H. Karasawa, R. Funayama, et al. 2019. "Cancer-Associated Fibroblasts Secrete Wnt2 to Promote Cancer Progression in Colorectal Cancer." *Cancer Medicine* 8: 6370–6382.

Anderson, N. M., and M. C. Simon. 2020. "The Tumor Microenvironment." *Current Biology* 30: R921–R925.

Baird, B. N., M. J. Schliekelman, Y. H. Ahn, et al. 2013. "Fibulin-2 Is a Driver of Malignant Progression in Lung Adenocarcinoma." *PLoS One* 8: e67054.

Barrett, T., S. E. Wilhite, P. Ledoux, et al. 2013. "NCBI GEO: Archive for Functional Genomics Data Sets—Update." *Nucleic Acids Research* 41: D991–D995.

Batra, R., T. J. Stark, A. E. Clark, et al. 2016. "RNA-Binding Protein CPEB1 Remodels Host and Viral RNA Landscapes." *Nature Structural & Molecular Biology* 23: 1101–1110.

Belhabib, I., S. Zaghdoudi, C. Lac, C. Bousquet, and C. Jean. 2021. "Extracellular Matrices and Cancer-Associated Fibroblasts: Targets for Cancer Diagnosis and Therapy?" *Cancers (Basel)* 13, no. 14: 3466. https://doi.org/10.3390/cancers13143466.

Bouchalova, P., and P. Bouchal. 2022. "Current Methods for Studying Metastatic Potential of Tumor Cells." *Cancer Cell International* 22: 394.

Brassart-Pasco, S., S. Brezillon, B. Brassart, L. Ramont, J. B. Oudart, and J. C. Monboisse. 2020. "Tumor Microenvironment: Extracellular Matrix Alterations Influence Tumor Progression." *Frontiers in Oncology* 10: 397.

Cai, X., C. Liu, T. N. Zhang, Y. W. Zhu, X. Dong, and P. Xue. 2018. "Down-Regulation of FN1 Inhibits Colorectal Carcinogenesis by Suppressing Proliferation, Migration, and Invasion." *Journal of Cellular Biochemistry* 119: 4717–4728.

Chiquet-Ehrismann, R., and R. P. Tucker. 2011. "Tenascins and the Importance of Adhesion Modulation." *Cold Spring Harbor Perspectives in Biology* 3, no. 5: a004960. https://doi.org/10.1101/cshperspect.a004960.

Chu, M. L., and T. Tsuda. 2004. "Fibulins in Development and Heritable Disease." *Birth Defects Research. Part C, Embryo Today* 72: 25–36.

Cox, T. R. 2021. "The Matrix in Cancer." *Nature Reviews. Cancer* 21: 217–238.

Danan-Gotthold, M., R. Golan-Gerstl, E. Eisenberg, K. Meir, R. Karni, and E. Y. Levanon. 2015. "Identification of Recurrent Regulated Alternative Splicing Events Across Human Solid Tumors." *Nucleic Acids Research* 43: 5130–5144.

de Vega, S., T. Iwamoto, and Y. Yamada. 2009. "Fibulins: Multiple Roles in Matrix Structures and Tissue Functions." *Cellular and Molecular Life Sciences* 66: 1890–1902.

de Visser, K. E., and J. A. Joyce. 2023. "The Evolving Tumor Microenvironment: From Cancer Initiation to Metastatic Outgrowth." *Cancer Cell* 41: 374–403.

DeLeon-Pennell, K. Y., T. H. Barker, and M. L. Lindsey. 2020. "Fibroblasts: The Arbiters of Extracellular Matrix Remodeling." *Matrix Biology* 91-92: 1–7.

Efthymiou, G., A. Saint, M. Ruff, Z. Rekad, D. Ciais, and E. Van Obberghen-Schilling. 2020. "Shaping up the Tumor Microenvironment With Cellular Fibronectin." *Frontiers in Oncology* 10: 641.

Fan, Y., Y. Hu, C. Yan, et al. 2018. "Loss and Gain of N-Linked Glycosylation Sequons due to Single-Nucleotide Variation in Cancer." *Scientific Reports* 8: 4322.

Giudice, J., Z. Xia, E. T. Wang, et al. 2014. "Alternative Splicing Regulates Vesicular Trafficking Genes in Cardiomyocytes During Postnatal Heart Development." *Nature Communications* 5: 3603.

Goldman, M. J., B. Craft, M. Hastie, et al. 2020. "Visualizing and Interpreting Cancer Genomics Data via the Xena Platform." *Nature Biotechnology* 38: 675–678.

Grassel, S., F. X. Sicot, S. Gotta, and M. L. Chu. 1999. "Mouse Fibulin-2 Gene. Complete Exon-Intron Organization and Promoter Characterization." *European Journal of Biochemistry* 263: 471–477.

Henke, E., R. Nandigama, and S. Ergun. 2019. "Extracellular Matrix in the Tumor Microenvironment and Its Impact on Cancer Therapy." *Frontiers in Molecular Biosciences* 6: 160.

Hetz, C., K. Zhang, and R. J. Kaufman. 2020. "Mechanisms, Regulation and Functions of the Unfolded Protein Response." *Nature Reviews. Molecular Cell Biology* 21: 421–438.

Hinkle, E. R., H. J. Wiedner, E. V. Torres, et al. 2022. "Alternative Splicing Regulation of Membrane Trafficking Genes During Myogenesis." *RNA* 28: 523–540.

Huang, X., Q. Ye, M. Chen, et al. 2019. "N-Glycosylation-Defective Splice Variants of Neuropilin-1 Promote Metastasis by Activating Endosomal Signals." *Nature Communications* 10: 3708.

Hulleman, J. D., and J. W. Kelly. 2015. "Genetic Ablation of N-Linked Glycosylation Reveals Two Key Folding Pathways for R345W Fibulin-3, a Secreted Protein Associated With Retinal Degeneration." *FASEB Journal* 29: 565–575.

Irimia, M., R. J. Weatheritt, J. D. Ellis, et al. 2014. "A Highly Conserved Program of Neuronal Microexons Is Misregulated in Autistic Brains." *Cell* 159: 1511–1523.

Kai, F., A. P. Drain, and V. M. Weaver. 2019. "The Extracellular Matrix Modulates the Metastatic Journey." *Developmental Cell* 49: 332–346.

Kim, S. K., S. Y. Kim, J. H. Kim, et al. 2014. "A Nineteen Gene-Based Risk Score Classifier Predicts Prognosis of Colorectal Cancer Patients." *Molecular Oncology* 8: 1653–1666.

Law, E. W., A. K. Cheung, V. I. Kashuba, et al. 2012. "Anti-Angiogenic and Tumor-Suppressive Roles of Candidate Tumor-Suppressor Gene, Fibulin-2, in Nasopharyngeal Carcinoma." *Oncogene* 31: 728–738.

Lee, H. S., Y. Qi, and W. Im. 2015. "Effects of N-Glycosylation on Protein Conformation and Dynamics: Protein Data Bank Analysis and Molecular Dynamics Simulation Study." *Scientific Reports* 5: 8926.

Ma, Y., M. Nenkov, D. C. Schroder, M. Abubrig, N. Gassler, and Y. Chen. 2021. "Fibulin 2 Is Hypermethylated and Suppresses Tumor Cell Proliferation Through Inhibition of Cell Adhesion and Extracellular Matrix Genes in Non-Small Cell Lung Cancer." *International Journal of Molecular Sciences* 22, no. 21: 11834. https://doi.org/10.3390/ijms222111834.

Mahajan, D., S. Kancharla, P. Kolli, et al. 2021. "Role of Fibulins in Embryonic Stage Development and Their Involvement in Various Diseases." *Biomolecules* 11: 685.

Mohan, V., A. Das, and I. Sagi. 2020. "Emerging Roles of ECM Remodeling Processes in Cancer." *Seminars in Cancer Biology* 62: 192–200.

Murphy, P. A., V. L. Butty, P. L. Boutz, et al. 2018. "Alternative RNA Splicing in the Endothelium Mediated in Part by Rbfox2 Regulates the Arterial Response to Low Flow." *eLife* 7: e29494.

Naba, A. 2023. "Ten Years of Extracellular Matrix Proteomics: Accomplishments, Challenges, and Future Perspectives." *Molecular & Cellular Proteomics* 22: 100528.

Naba, A., K. R. Clauser, H. Ding, C. A. Whittaker, S. A. Carr, and R. O. Hynes. 2016. "The Extracellular Matrix: Tools and Insights for the "Omics" Era." *Matrix Biology* 49: 10–24.

Pan, T. C., T. Sasaki, R. Z. Zhang, R. Fassler, R. Timpl, and M. L. Chu. 1993. "Structure and Expression of Fibulin-2, a Novel Extracellular Matrix Protein With Multiple EGF-Like Repeats and Consensus Motifs for Calcium Binding." *Journal of Cell Biology* 123: 1269–1277.

Peixoto, A., M. Relvas-Santos, R. Azevedo, L. L. Santos, and J. A. Ferreira. 2019. "Protein Glycosylation and Tumor Microenvironment Alterations Driving Cancer Hallmarks." *Frontiers in Oncology* 9: 380.

Pelka, K., M. Hofree, J. H. Chen, et al. 2021. "Spatially Organized Multicellular Immune Hubs in Human Colorectal Cancer." *Cell* 184: 4734–4752.e20.

Pickup, M. W., J. K. Mouw, and V. M. Weaver. 2014. "The Extracellular Matrix Modulates the Hallmarks of Cancer." *EMBO Reports* 15: 1243–1253.

Pinho, S. S., and C. A. Reis. 2015. "Glycosylation in Cancer: Mechanisms and Clinical Implications." *Nature Reviews. Cancer* 15: 540–555.

Popov, M., J. Li, and R. A. Reithmeier. 2000. "Resolution of Glycoproteins by a Lectin Gel-Shift Assay." *Analytical Biochemistry* 279: 90–95.

Rafaeva, M., and J. T. Erler. 2020. "Framing Cancer Progression: Influence of the Organ- and Tumour-Specific Matrisome." *FEBS Journal* 287: 1454–1477.

Rekad, Z., V. Izzi, R. Lamba, D. Ciais, and E. Van Obberghen-Schilling. 2022. "The Alternative Matrisome: Alternative Splicing of ECM Proteins in Development, Homeostasis and Tumor Progression." *Matrix Biology* 111: 26–52.

Ryan, M., W. C. Wong, R. Brown, et al. 2016. "TCGASpliceSeq a Compendium of Alternative mRNA Splicing in Cancer." *Nucleic Acids Research* 44: D1018–D1022.

Sasaki, T., W. Gohring, T. C. Pan, M. L. Chu, and R. Timpl. 1995. "Binding of Mouse and Human Fibulin-2 to Extracellular Matrix Ligands." *Journal of Molecular Biology* 254: 892–899.

Sasaki, T., K. Mann, H. Wiedemann, et al. 1997. "Dimer Model for the Microfibrillar Protein Fibulin-2 and Identification of the Connecting Disulfide Bridge." *EMBO Journal* 16: 3035–3043.

Sasaki, T., H. Wiedemann, M. Matzner, M. L. Chu, and R. Timpl. 1996. "Expression of Fibulin-2 by Fibroblasts and Deposition With Fibronectin Into a Fibrillar Matrix." *Journal of Cell Science* 109, no. Pt 12: 2895–2904.

Schjoldager, K. T., Y. Narimatsu, H. J. Joshi, and H. Clausen. 2020. "Global View of Human Protein Glycosylation Pathways and Functions." *Nature Reviews. Molecular Cell Biology* 21: 729–749.

Schneider, C. A., W. S. Rasband, and K. W. Eliceiri. 2012. "NIH Image to ImageJ: 25 Years of Image Analysis." *Nature Methods* 9: 671–675.

Sebestyen, E., M. Zawisza, and E. Eyras. 2015. "Detection of Recurrent Alternative Splicing Switches in Tumor Samples Reveals Novel Signatures of Cancer." *Nucleic Acids Research* 43: 1345–1356.

Sicot, F. X., T. Tsuda, D. Markova, et al. 2008. "Fibulin-2 Is Dispensable for Mouse Development and Elastic Fiber Formation." *Molecular and Cellular Biology* 28: 1061–1067.

Spada, S., A. Tocci, F. Di Modugno, and P. Nistico. 2021. "Fibronectin as a Multiregulatory Molecule Crucial in Tumor Matrisome: From Structural and Functional Features to Clinical Practice in Oncology." *Journal of Experimental & Clinical Cancer Research* 40: 102.

Sun, Y., C. Zhao, Y. Ye, et al. 2020. "High Expression of Fibronectin 1 Indicates Poor Prognosis in Gastric Cancer." *Oncology Letters* 19: 93–102.

Timpl, R., T. Sasaki, G. Kostka, and M. L. Chu. 2003. "Fibulins: A Versatile Family of Extracellular Matrix Proteins." *Nature Reviews. Molecular Cell Biology* 4: 479–489.

Trapnell, C., B. A. Williams, G. Pertea, et al. 2010. "Transcript Assembly and Quantification by RNA-Seq Reveals Unannotated Transcripts and Isoform Switching During Cell Differentiation." *Nature Biotechnology* 28: 511–515.

Vaes, N., S. L. Schonkeren, G. Rademakers, et al. 2021. "Loss of Enteric Neuronal Ndrg4 Promotes Colorectal Cancer via Increased Release of Nid1 and Fbln2." *EMBO Reports* 22: e51913.

Viloria, K., and N. J. Hill. 2016. "Embracing the Complexity of Matricellular Proteins: The Functional and Clinical Significance of Splice Variation." *Biomolecular Concepts* 7: 117–132.

Wang, J., J. Lee, D. Liem, and P. Ping. 2017. "HSPA5 Gene Encoding Hsp70 Chaperone BiP in the Endoplasmic Reticulum." *Gene* 618: 14–23.

Wasser, C. R., I. Masiulis, M. S. Durakoglugil, et al. 2014. "Differential Splicing and Glycosylation of Apoer2 Alters Synaptic Plasticity and Fear Learning." *Science Signaling* 7: ra113.

Winkler, J., A. Abisoye-Ogunniyan, K. J. Metcalf, and Z. Werb. 2020. "Concepts of Extracellular Matrix Remodelling in Tumour Progression and Metastasis." *Nature Communications* 11: 5120.

Woodard, D. R., E. Nakahara, and J. D. Hulleman. 2021. "Clinically-Identified C-Terminal Mutations in Fibulin-3 Are Prone to Misfolding and Destabilization." *Scientific Reports* 11: 2998.

Xia, S., C. Wang, E. L. Postma, Y. Yang, X. Ni, and W. Zhan. 2017. "Fibronectin 1 Promotes Migration and Invasion of Papillary Thyroid Cancer and Predicts Papillary Thyroid Cancer Lymph Node Metastasis." *Oncotargets and Therapy* 10: 1743–1755.

Xiao, J., W. Yang, B. Xu, et al. 2018. "Expression of Fibronectin in Esophageal Squamous Cell Carcinoma and Its Role in Migration." *BMC Cancer* 18: 976.

Xu, C., and D. T. Ng. 2015. "Glycosylation-Directed Quality Control of Protein Folding." *Nature Reviews Molecular Cell Biology* 16: 742–752.

Ye, Y., R. Zhang, and H. Feng. 2020. "Fibronectin Promotes Tumor Cells Growth and Drugs Resistance Through a CDC42-YAP-Dependent Signaling Pathway in Colorectal Cancer." *Cell Biology International* 44: 1840–1849.

Yi, C. H., D. J. Smith, W. W. West, and M. A. Hollingsworth. 2007. "Loss of Fibulin-2 Expression Is Associated With Breast Cancer Progression." *American Journal of Pathology* 170: 1535–1545.

Yi, W., E. Xiao, R. Ding, P. Luo, and Y. Yang. 2016. "High Expression of Fibronectin Is Associated With Poor Prognosis, Cell Proliferation and Malignancy via the NF-kappaB/p53-Apoptosis Signaling Pathway in Colorectal Cancer." *Oncology Reports* 36: 3145–3153.

Zhang, H., D. Hui, and X. Fu. 2020. "Roles of Fibulin-2 in Carcinogenesis." *Medical Science Monitor: International Medical Journal of Experimental and Clinical Research* 26: e918099.

Zhang, X., L. Duan, Y. Zhang, H. Zhao, X. Yang, and C. Zhang. 2020. "Correlation of Fibulin-2 Expression With Proliferation, Migration and Invasion of Breast Cancer Cells." *Oncology Letters* 20: 1945–1951.

Supporting Information

Additional supporting information can be found online in the Supporting Information section.